Available online at www.sciencedirect.com
SCIENCE DIRECT®
International Journal of Machine Tools & Manufacture 44 (2004) 1205–1214
INTERNATIONAL JOURNAL OF MACHINE TOOLS & MANUFACTURE DESIGN, RESEARCH AND APPLICATION
www.elsevier.com/locate/ijmactool

Joining of Al 6061 alloy to AISI 1018 steel by combined effects of fusion and solid state welding

C.M. Chen, R. Kovacevic *

Department of Mechanical Engineering, Research Center for Advanced Manufacturing, Southern Methodist University, 1500 International Parkway, Suite 100, Richardson, TX 75081, USA

Received 28 November 2003; received in revised form 17 March 2004; accepted 23 March 2004

Abstract

The joining of a 6-mm thickness Al 6061 to AISI 1018 steel has been performed by the combined effects of fusion and solid state welding. The process is derived from friction stir welding (FSW) but with an adjustable offset of the probe location with respect to the butt line. Metallographic studies by optical microscopy, electron probe microscopy, and the utilization of the X-ray diffraction technique have been conducted. It was found that the intermetallic phases $Al_{13}Fe_4$ and Al_5Fe_2 exist in the weld zone. The tool was significantly worn during welding and is broken after traveling 100 mm at a rotational speed of 917 rpm. The wear of the tool significantly affects the structure of the weld, and the tool breakage was detected by the incorporated acoustic emission (AE) sensors. It appears that the joining of an Al 6061 alloy to AISI 1018 steel with a sound heterogeneous weld microstructure is feasible using this process, and the tool breakage can be detected by the AE sensing technique.

Keywords: Fusion and solid state welding; Joining of steel to aluminum; Heterogeneous weld microstructure; Tool breakage detection; Intermetallic phases; Acoustic emission

1. Introduction

The driving force for joining aluminum and steel arises from the need for weight savings, thus essentially, from a need for energy-efficiency in automobile industry [1,2], and the requirement for chemical plants and cryogenic applications. However, the dissimilar combination of aluminum and steel is generally difficult in virtue of the wide difference in their thermal and mechanical properties, and the tendency to form brittle intermetallic compounds [3,4]. Conventional fusion welding methods, such as arc and laser heating have been used to join aluminum and steel [2,5,6]; however, the poor seam surface of the weld and the formation of porosity in the weld hinder the practical applications of these two techniques. Friction welding has been proven practical to eliminate the formation of the intermetallic phases and to form a sound weld [3,7,8], but this method is usually used for joining cylindrical parts. As a newly emerging technology, friction stir welding (FSW), which has been widely applied in the industry for joining aluminum alloys and is expanding its application in joining steels [9,10], is expected to provide a practical solution for joining aluminum–steel.

Watanabe et al. [11] reported the joining of steel to an aluminum alloy 2-mm thick by interface-activated adhesion welding with a preliminarily satisfactory joint, but not much detail about microstructures was shown. In welding dissimilar materials, especially with a high difference in melting points, the microstructure evolution and material flow behavior are basic issues for the weldability study. Among the main concerns are the severity of tool wear encountered in welding high-melting-point materials and the monitoring of the tool condition, especially the tool breakage. This paper is a feasibility study for joining Al 6061 alloy to AISI 1018 steel that is 6-mm thick. An additional goal of this project is to develop a methodology of monitoring tool breakage in real time.

* Corresponding author. Tel.: +1-214-768-4873; fax: +1-214-768-0812.
E-mail address: kovacevi@seas.smu.edu (R. Kovacevic).

0890-6955/$ - see front matter © 2004 Elsevier Ltd. All rights reserved.
doi:10.1016/j.ijmachtools.2004.03.011

2. Experimental details

Two plates of Al 6061-T6 and cold-rolled AISI 1018 steel 6 mm thick, and 50 and 25 mm wide, respectively, were friction stir welded along the butted joint as shown in Fig. 1. The steel was in the retreating side, the aluminum was in the advancing side, and their nominal compositions are given in Table 1. The tool made of tool steel was selected in this experiment. It is evident that this selection is not an optimal tool material for welding steel, since wear-resistant materials such as tungsten- and molybdenum-based alloys are thought better for the application [9]; however, it provided an accelerated tool-wear conditions in the contact with the steel. The tool consists of a shoulder with a diameter of 24 mm and a probe with a diameter of 5.5 mm, as shown in Fig. 2. The tool traverse and rotational speeds are set at 140 mm/min and 914 rpm, respectively. Preliminary wear test showed that the probe decreases 0.64 mm in diameter after the tool traverses 70 mm along the welding direction.

Four preliminary experiments are conducted to determine the appropriate offset of the probe to the butt line. One experiment was performed when the tool probe was entirely immersed into aluminum, the offset = 2.75 mm; the second experiment was conducted with the probe entirely immersed in steel, offset = −2.75 mm; the third experiment was carried out with the probe plunged into the butt line, offset = 0 mm; and the fourth experiment was accomplished with +1 mm offset of probe to the butt line, as shown in Fig. 3a–d, respectively. With the offset of −2.75 and +2.75 mm, the joint between the aluminum alloy and the steel is generated only by the shoulder action, and joint is too weak. With the offsets of 0 mm, the friction between the faying surface of the steel and the probe generates enough heat to initiate a strong reaction between the steel and the aluminum alloys that subsequently produces a large amount of intermetallics. The offset of the location of tool with respect to the butt line was adjusted at +1 mm (the optimal offset requires further study) and a sound joint was determined by eye examination. In this paper, a metallographic study of the sound joint is performed with a +1-mm offset.

During welding, an on-line acoustic emission (AE) monitoring system was used to detect the tool wear conditions. Two static AE sensors were placed on the top of the plates symmetrically with respect to the joint line. The generated AE signature during welding was picked up by the AE sensors, progressively amplified through two preamplifiers with a selection of a 40-dB gain and a 20-kHz high-pass filter, and transmitted to the signal processor.

Weld temperature was measured by two 0.5-mm K-type thermocouples, each of which is embedded at the half-thickness point opposite one another with a distance of 3.5 mm to the joint line in the steel and 4.5 mm in the aluminum. Cross-sections of the weld were taken at distances of 20, 45, 80, and 120 mm from to the weld starting point, and progressively polished and etched with Keller's reagent before optical metallographic examination. A scanning electron microscope (SEM) equipped with an energy dispersive X-ray spectroscopy (EDS) apparatus was used to examine the more delicate structure formed in the nugget and for compositional microanalysis. An X-ray diffractometer with CuK_{α} was further used to identify the phases formed in the nugget. During the X-ray measurement, in order to increase the detection resolution, a mask made of graphite sheet was used to block out the unwanted area. The Vickers microhardness measure-

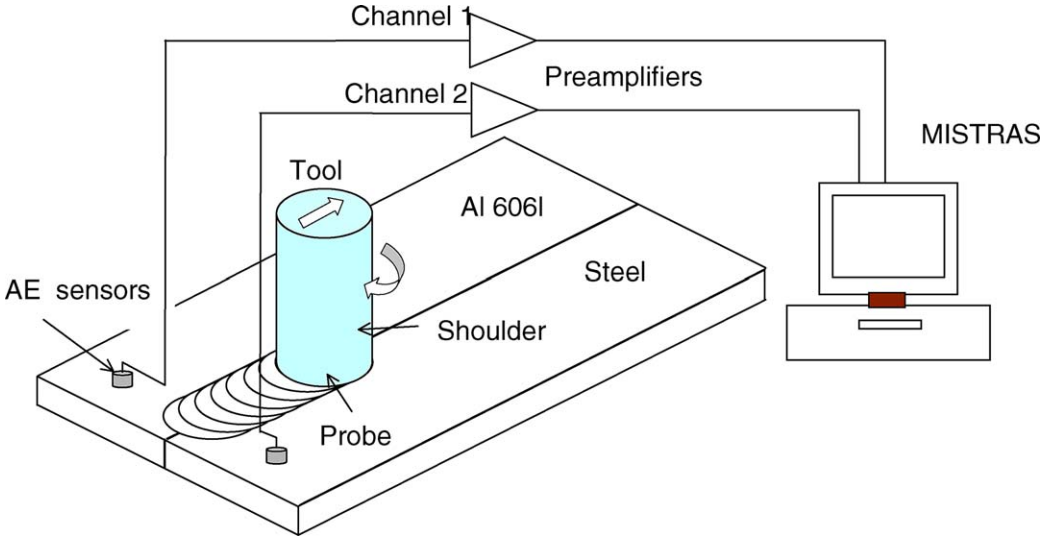

Fig. 1. Scheme of AE monitoring set-up.

Table 1
Nominal chemical composition of welded materials and tool (wt.%)

Al 6061-T6						
Si	Mg	Cu	Fe	Cr	Mn	Al
0.4–0.8	0.8–1.2	0.15–0.4	<0.7	0.04–0.35	<0.15	Bal.
AISI 1018						
C	Mn	P	S			Fe
0.14–0.2	0.6–0.9	<0.04	<0.05			Bal.
Tool						
C	V			Cr	Mo	Fe
0.80	2.75			7.5	1.30	Bal.

Fig. 2. Picture of tool feature.

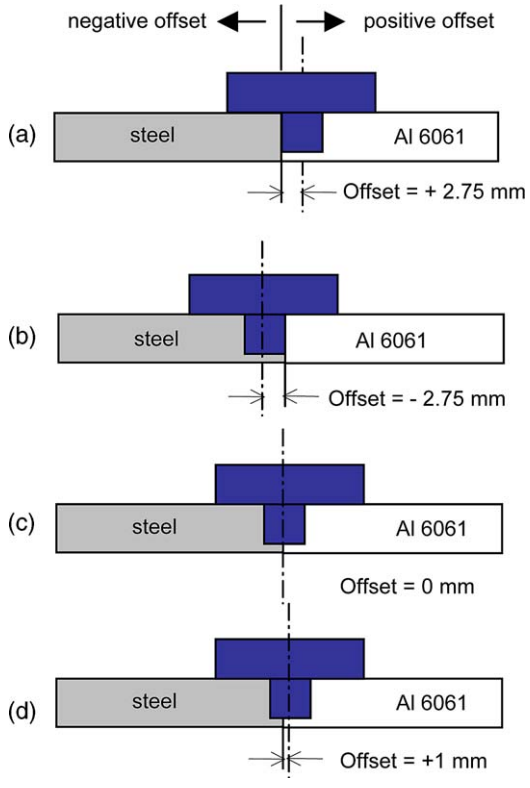

Fig. 3. Scheme of relative location of probe and the butt line of the welded plates.

ments were also performed at the half-thickness point across the weld zone prior to etching, using a 50-g load and a 15-s dwelling time.

3. Results and discussion

3.1. Weld quality and the temperature history

The weld structure appears good in the portion measured between 25- and 70-mm marks from the weld starting point, shown as the B region in Fig. 4, as there is no porosity visible on the top and bottom of the weld. In the 25-mm long portion of the weld from the starting point (region A), there are numerous holes and pores exposed on the top of the weld concentrated along the centerline, which may be due to the unstable welding state and insufficient heat accumulation in the weld zone in the initial welding stage. In the portion of the weld between 70 and 100 mm from the starting point (region C), there is a cluster of discrete pores dispersed along the butt line at the bottom of the weld, which is evidently caused by the wear of the probe. Probe breakage was determined to occur at a distance of 100 mm from the starting point based on a visual examination of the bottom side of the weld as shown in Fig. 4.

The temperature and heating/cooling rate of both plates of Al 6061 and AISI 1018 steel were measured, and their profiles are shown in Fig. 5. The maximum measured temperature and heating rate for the aluminum alloy are 491 °C and 90 °C/s, respectively, and the maximum measured temperature and the heating rate for the steel are 631 °C and 175 °C/s, respectively. Considering the thermal properties of the materials, it is calculated that the energy input into the steel is around three times that of the aluminum alloy at a rotational speed of 914 rpm and a traverse speed of 140 mm/min. The maximum measured cooling rates for the aluminum alloy and steel are 21 and 51 °C/s, respectively. The offset of the instances when the maximum temperatures in the two materials occur is due to the poorer heat conductivity of the steel compared to the aluminum.

A simulation of the temperature by using a finite element analysis was conducted based on the assumption that the thermal resistance between the tool and the welded materials is zero. The convection coefficients on the welded plate sides were adjusted so that the simulation results at the two thermocouple points match closely to the measured ones. Fig. 6 gives the simulated temperature distribution at the half-thickness which shows that the steel–probe interface temperature and Al–probe temperature are 665 and 532 °C, respectively.

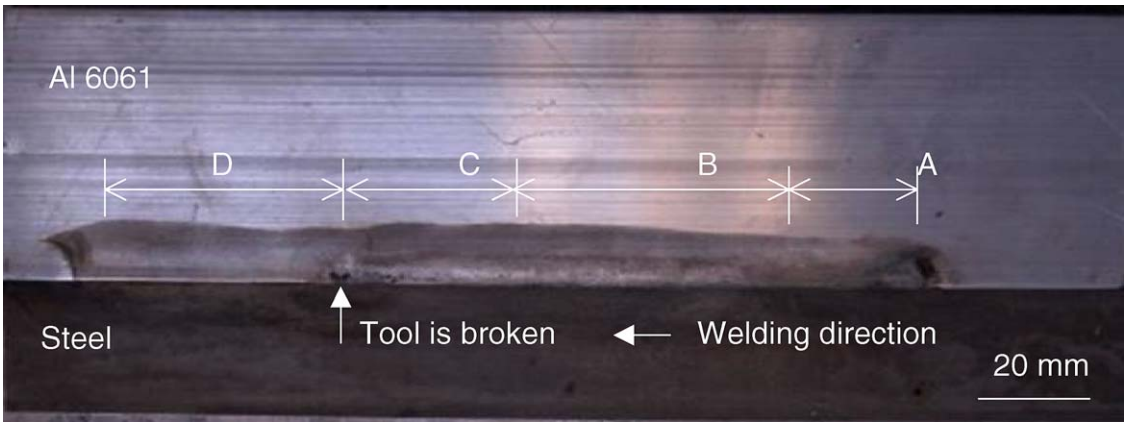

Fig. 4. Backside view of the welded Al 6061–steel plates showing the probe breakage after the tool travels 100 mm.

3.2. Structures and microhardness

For comparison, Fig. 7 shows the macrostructure of the cross-sections of the weld at various distances from the starting point of 20, 45, 80, and 120 mm. It is obvious that the nuggets are filled with steel platelets or blocks sheared off from the steel plate, which is believed to be a result of the abrasion wear and shearing by the tool. The dimension of the nuggets and the number of the steel platelets or blocks shown in Fig. 7(a)–(c) show a decreasing trend indicating evidence of tool wear during FSW. A relatively smaller number of steel platelets or blocks are present at the aluminum side. Fig. 7(d) indicates a tool breakage and shows a plate section of which a fourth of the thickness is welded barely underneath the shoulder, resulting from the friction and extrusion between the shoulder and the welded plates after the probe is broken.

It can be noted from the nugget micrograph shown in Fig. 7(a) that a cluster of segregated steel chunks are mainly distributed in the steel side of the nugget, which is attributed to the abrasive wear between the tool and the cold plates at the initial welding stage. Compared to the findings in Fig. 7(a), the nugget shown in Fig. 7(b) displays a sound microstructure with a more uniformly distributed steel platelet. Excessive wear of the tool causes the presence of holes at the top of the weld and along the bottom edge of the nugget as shown in Fig. 7(c). From all the micrographs shown in Fig. 7, the steel edge adjacent to the nugget reveals abrasive wear by the rotating tool and appears to have

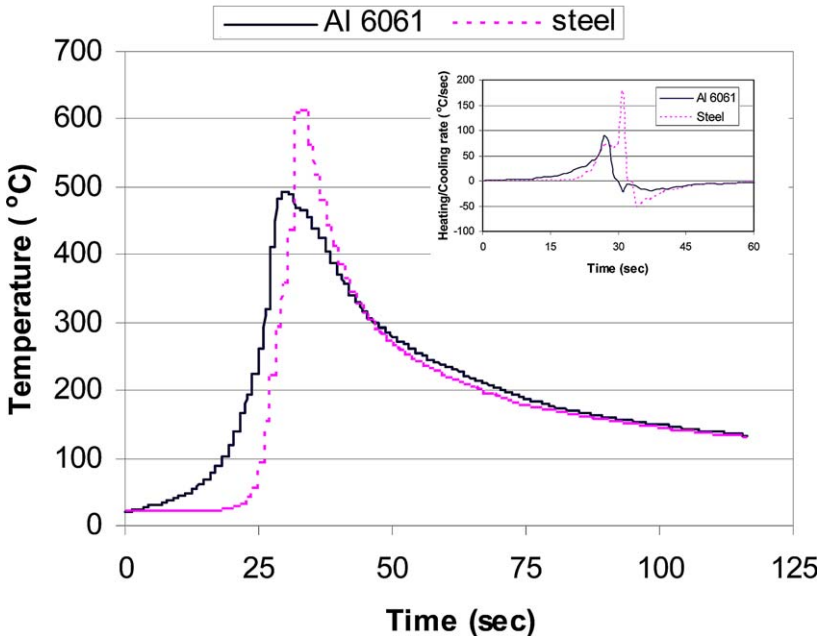

Fig. 5. Temperature–time profiles for the Al 6061 and steel at distances of 4.5 and 3.5 mm from the butt line, respectively. The in-set shows the corresponding heating/cooling rates of the materials.

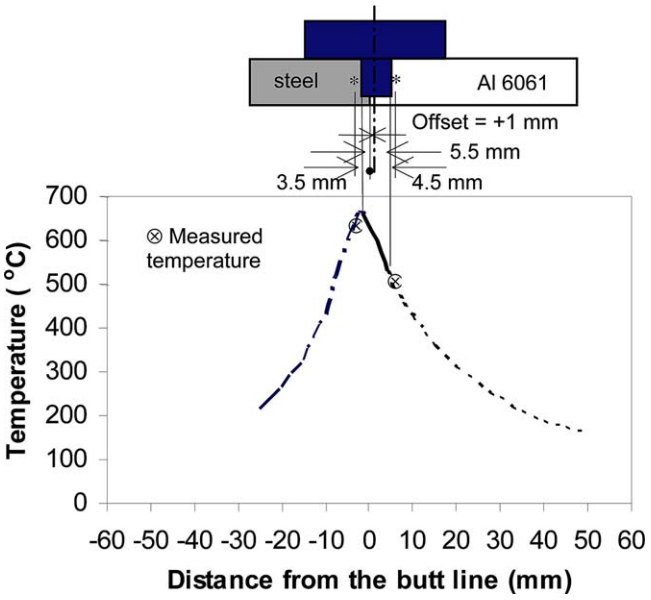

Fig. 6. Temperature simulation result of steel–Al 6061 weldment with a tool offset of +1 mm to the butt line.

a "saw" shape, which becomes more pronounced when approaching the top surface. It is noted that the "saw" structure still appears in Fig. 7(d) after tool breakage. It is believed that the "saw" structure is caused by the shearing force exerted by the tool, especially by the shoulder, as a relatively smooth edge occurs at the bottom side of the nugget.

Furthermore, an in-depth examination of the microstructure is based on the sound weld with no holes and no apparent defects in the nugget shown in Fig. 8(b). Fig. 8 shows the magnified images of the nugget zone corresponding to the locations A and B in Fig. 7(b). The base steel typically comprises of equiaxed grains containing pearlite and ferrite. A layer of fine structure is formed in the base steel adjacent to the edge of the nugget zone, which is believed to be caused by the dynamic recrystallization of the strained and/or deformed zone [12], and high cooling rate through the passage of aluminum after tool traversing. Relatively coarse grains are observed in the region beyond the fine structured layer due to the slow cooling rate. The "saw" structure shown in Fig. 8(b) encompasses an aluminum alloy with intermetallic compounds formed in between.

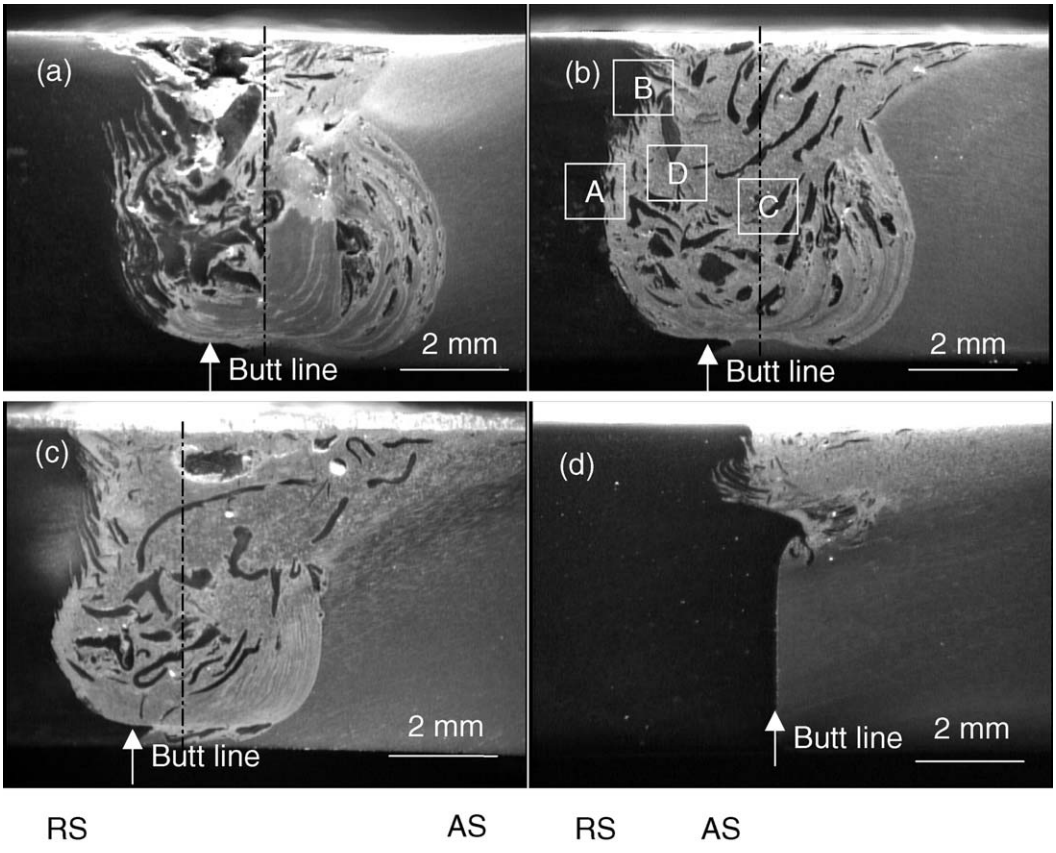

Fig. 7. Optical microstructure of the weld cross-sections with various travel distances of (a) 20 mm, (b) 45 mm, (c) 80 mm, and (d) 120 mm in the corresponding regions A, B C, and D indicated in Fig. 2, respectively (RS—retreating side, AS—advancing side, the dotted line represents the location of weld center with a offset of +1 mm to the butt line).

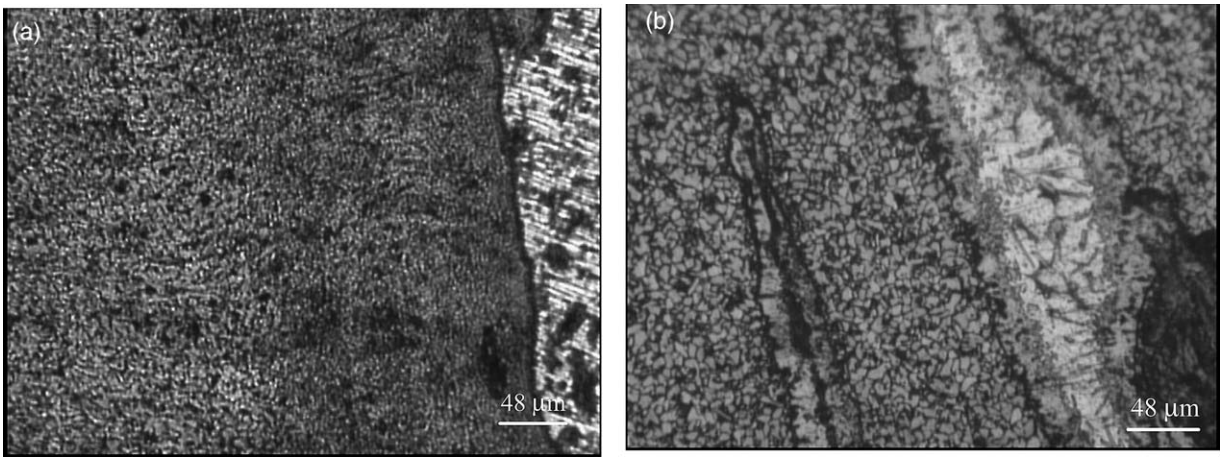

Fig. 8. Optical microstructure of base steel near the edge of the nugget showing (a) a layer of fine grain structure (corresponds to the location A in Fig. 6(b) and (b)) "saw" structure which encompasses with aluminum alloy (corresponds to location B in Fig. 6b).

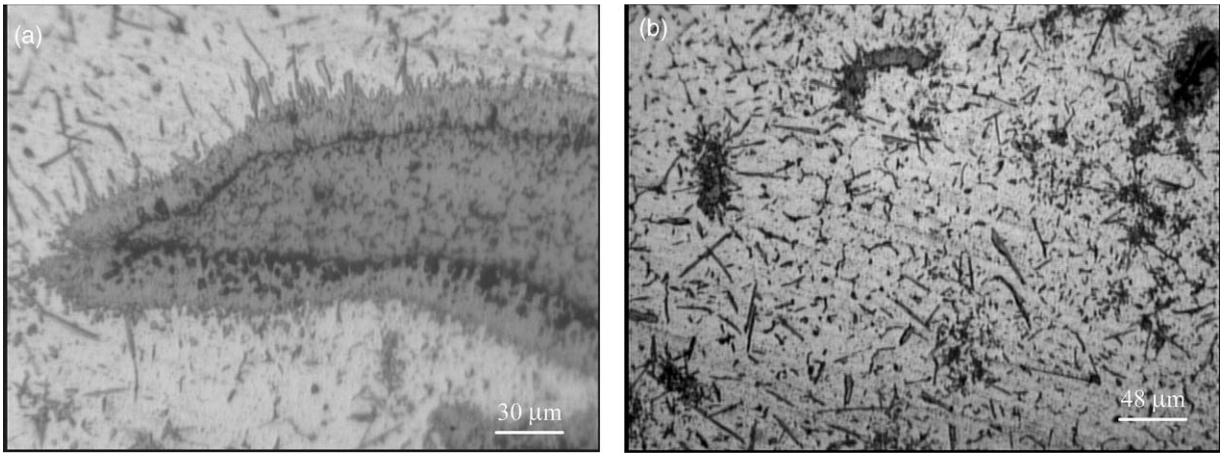

Fig. 9. Optical view of (a) a typical steel platelet and (b) the Al 6061 matrix in the nugget zone at the steel side.

In the nugget zone, a significantly heterogeneous structure reveals the complex thermomechanical process and consolidation process during stirring. Fig. 9(a) shows the magnified view of a platelet encompassed in the nugget at the steel side. It is seen that a layer of intermetallic compound encircles the platelet, which is the reactive product of the aluminum and steel. In the region around the platelet as shown in Fig. 9a, b, a large amount of needle-like compounds are dispersed in the base aluminum, which seem detached from the intermetallic layer due to the extreme stirring action in the nugget zone. In some regions of the nugget, the base aluminum is dispersed with intermetallic compounds with petal or needle shapes, which are mostly typical precipitations from the melt.

The petal- and needle-like precipitations observed in the nugget at the steel side reveal that melting occurs during welding, which can be further proved by the temperature measurement and simulation results shown in Figs. 5 and 6. The temperature at the probe–steel interface could be as high as 675 °C during welding. Based on the Al–Fe phase diagram given in Fig. 10 [13] and the melting point of Al 6061 in the range

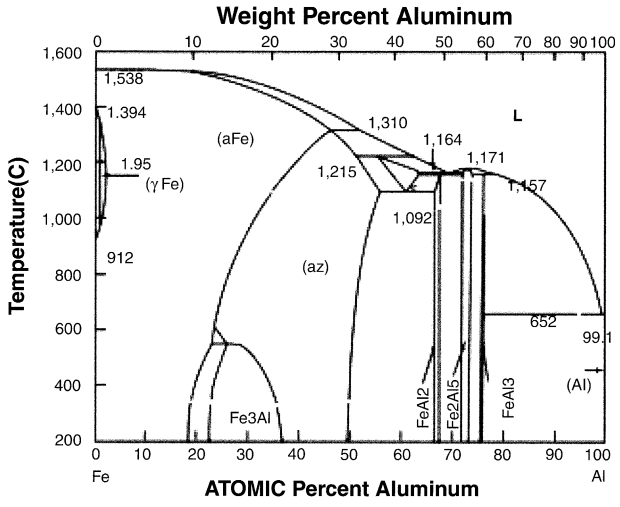

Fig. 10. Phase diagram of Al–Fe.

582–652 °C, the melting of the base aluminum should have happened at the connection of the Al 6061 with the steel side. Moreover, it is possible that the rotating tool will transfer the melt material to the central nugget region.

An SEM equipped with an EDS is also used for the observation of the phase shape and the analysis of its composition. Fig. 11(a) shows a stacked structure of a platelet near the aluminum side. The atom ratio in the A layer is Al : Fe = 3.41, and the phase is most likely to be $Al_{13}Fe_4$ of which the atom ratio is Al : Fe = 3.25. In layer B, Al : Fe = 1.46. Probably, the phase in this region is Al_5Fe_4, which needs to be further verified. X-ray diffraction was also performed, and the result that is shown in Fig. 12 indicates that intermetallic phases $Al_{13}Fe_4$ and Al_5Fe_2 exist in the weld zone. The two intermetallic compounds were also found to exist in friction welded Al-304 stainless steel [8,14].

The microhardness measurement for samples corresponding to Fig. 7(a), (b) is profiled in Fig. 13. A significant oscillation of the hardness value in the nugget zone is revealed, which is attributed to the heterogeneous structure of the aluminum, steel, and formed intermetallic compounds in the nugget zone. The peaks of hardness are related to the existence of the intermetallic compound. In the base steel near the nugget zone, a high hardness value is related to the formation of the fine structure in this region as shown in Fig. 8(a), and the decrease in hardness away from this layer is related to the coarse grain structure in the corresponding

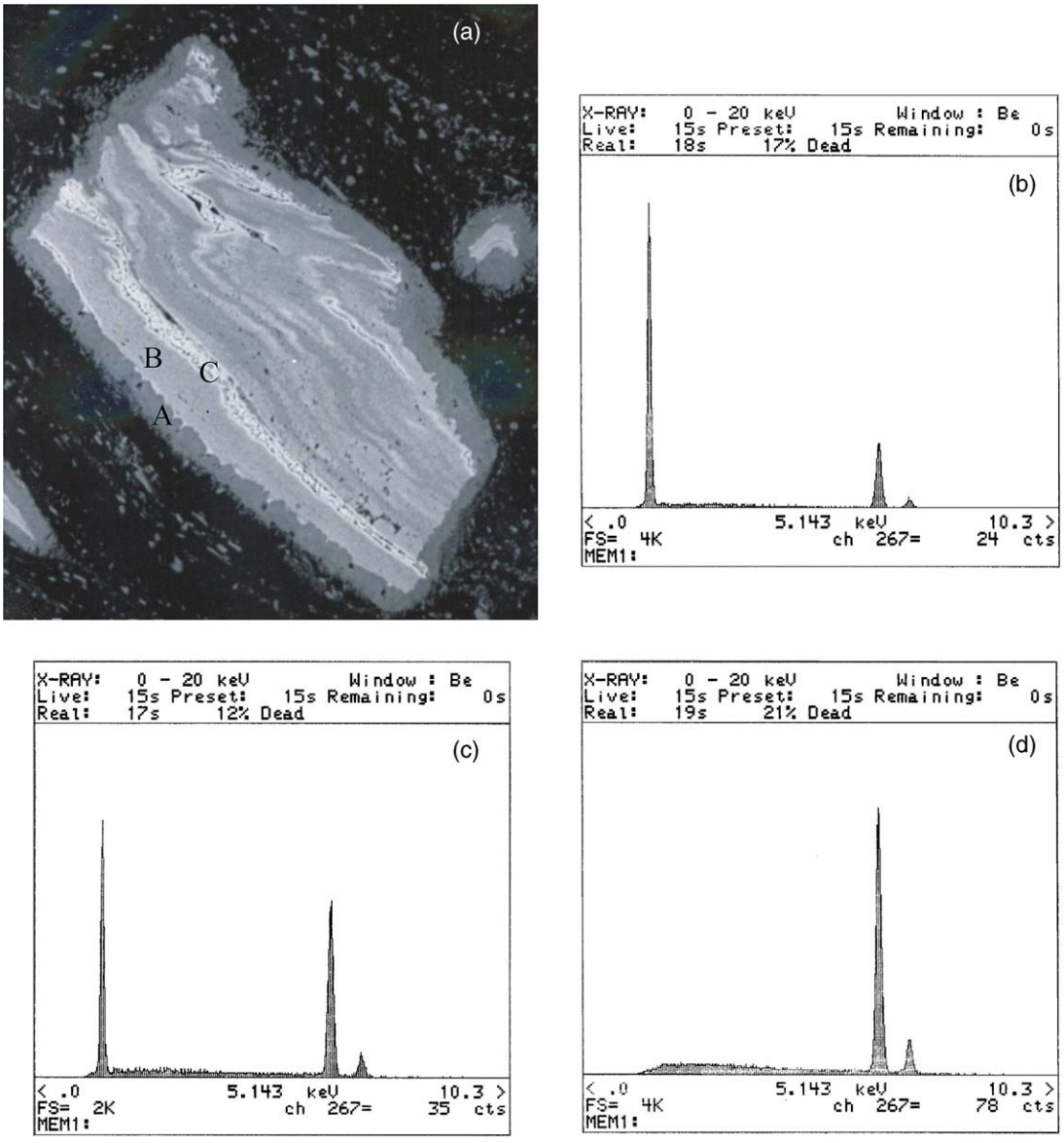

Fig. 11. (a) The electron backscatter image for a platelet existing in the nugget shows a stacked layer structure inside; the EDS spectra for the positions (a) A, (b) B, and (c) C labeled in (a) shows the possible existence of $Fe_{13}Al_4$, Fe_5Al_2, and base steel, respectively.

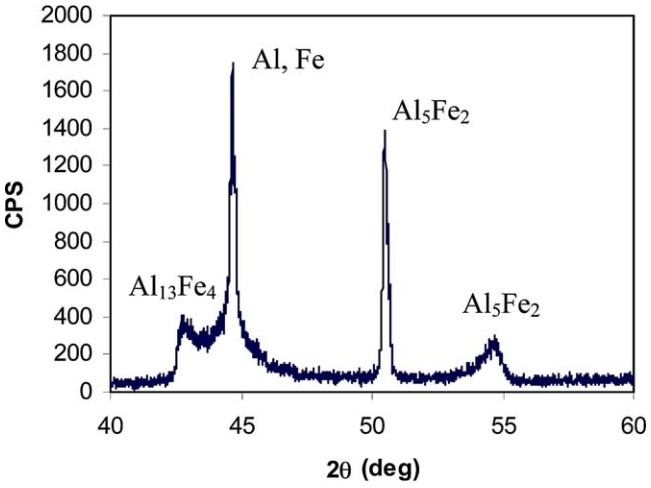

Fig. 12. XRD spectrum showing the existence of $Al_{13}Fe_4$ and Al_5Fe_2 in the nugget.

region. In the base aluminum, no evident decrease in hardness is observed in the direction away from the nugget boundary compared with the friction stir welded aluminum alloys in which the heat-affected zone usually has less hardness [15].

3.3. Weld quality and tool breakage monitoring

AE monitoring is one of the most sensitive techniques used for real-time detection of cutting tool wear and tool breakage [16]. A wavelet transform (WT), in which the band energy at each scale that corresponds to a specific band of frequency represents a different bandwidth is more appropriate for the analysis of complex signals such as transient and abrupt changes that are generally the symptoms of sudden changes of the process. WT is expected to be used for the extraction of features in tool breakage detection.

The details of WT transform can be found in Ref. [17], and the related WT transform results are shown as an aerial view in Fig. 14(a) and as contour map in Fig. 14(b). The difference in the band energy profile and contour map before and after the tool breakage is easily recognized at a glance, indicated at arrows in Fig. 14.

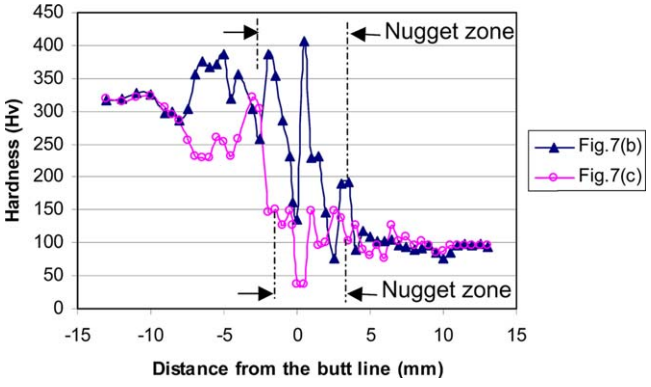

Fig. 13. Microhardness profiles in the mid-thickness of FSW cross-sections corresponding to Fig. 6(b) and (c), respectively.

More details of WT are shown in Fig. 15 for Channel 1 (Al side). It is seen that during the initial welding of region A, there are several sparse spikes that appear at every scale, which may be related to the formation of holes in the nugget as shown in Fig. 7(a). A small amount of spikes with less amplitude in region B corresponds to the sound weld structure shown in Fig. 7(b). It is also demonstrated by microstructural examination that the holes and "kiss" (lack of strong bond between the nugget edge and the bottom edge) defects exist in the nugget edge of samples taken from region C of the weld shown in Fig. 4, which may explain the energy spikes in region C of Fig. 15. After tool breakage, a periodic oscillation of energy (region D) reveals an evident difference from the features before the tool breakage happens.

The results in this study demonstrate the feasibility of using the AE technique for the monitoring of weld quality and tool breakage. It should be noted that the spikes reveal mostly the formation of defects in the welds or sudden changes in the process state. In the author's previous experiments for monitoring the FSW process with pre-designed holes in the welded plates, the big change of AE energy indicated a significant change in the interaction between the tool and welded plates [17].

These preliminary experiments show that joining Al to steel is done through a combination of fusion and solid state welding. It should be pointed that although FSW is usually regarded as a purely solid state welding method, welding of dissimilar materials especially those with a big difference in melting points will generate localized fusion in the stir zone. The combined effect of fusion and stir is expected to help in homogenizing the heterogeneous structure of the weld zone. The optimization of the welding parameters is in progress, and tests of mechanical properties such as tensile strength, fatigue, and corrosion resistance performance of a steel-to-aluminum alloy weld remain to be further investigated.

4. Conclusions

This results of the study lead to the following conclusions:

1. FSW can be used to joint 6061 aluminum alloy to mild steel through the combined effects of fusion and solid state welding.
2. Intermetallic compounds $Al_{13}Fe_4$, Al_5Fe_2 are found to exist in the nugget zone.

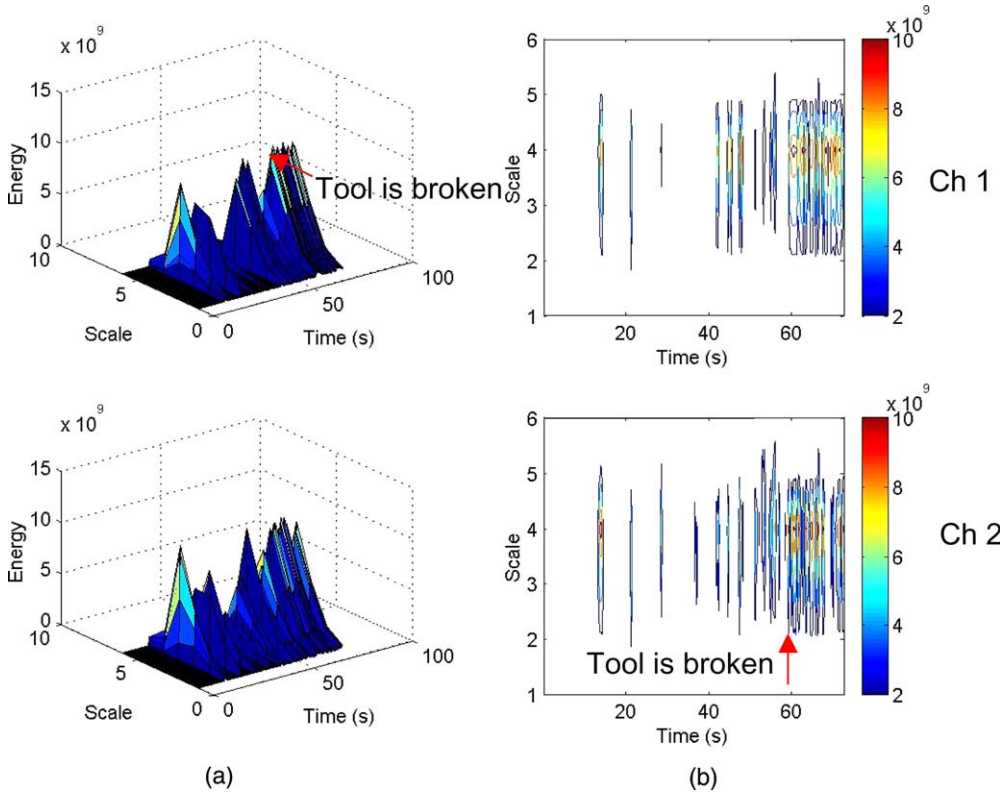

Fig. 14. (a) The three-dimensional profile and (b) contour map of WT for the welding process with tool breakage.

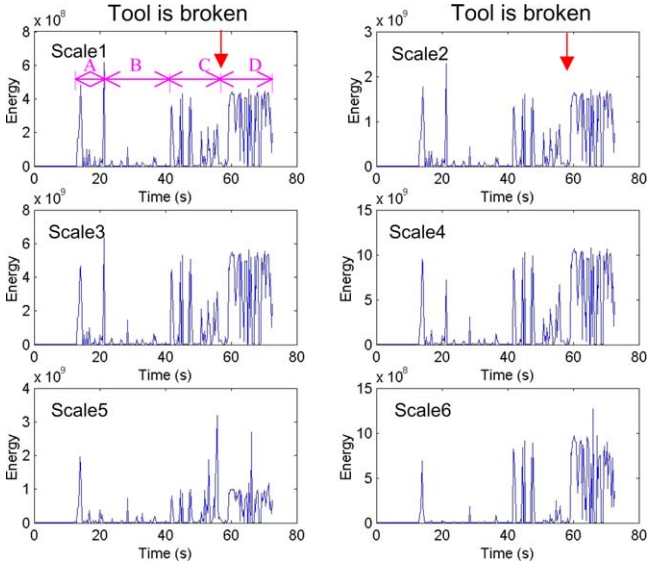

Fig. 15. Plots of band energy vs. time at different scales for the welding process with tool breakage (Channel l); the band energy features of regions A, B, C and D correspond to the welding regions A, B, C, and D indicated in Fig. 3, respectively.

3. The tool wear causes the formation of hole, and lessen homogenization of structure in the weld zone.
4. The AE technique is a sensitive means for monitoring the weld quality and the detection of tool breakage.

Acknowledgements

This work was financially supported by the US Department of Education, Grant No. P200A80806-98, Brown Foundation, Houston, TX, and SMU's Research Center for Advanced Manufacturing, Richardson, TX. Assistance by Mr. Michael Valant, research engineer during the experiments, and Dr. W.F. Jiang in preparing samples is gratefully acknowledged.

References

[1] G. Kobe, Aluminum/steel welding, Automotive Industries 7 (1994) 44.
[2] S. Ramasamy, Drawn arc stud welding: Crossing over from steel to aluminium, Welding Journal 2 (2003) 35–39.
[3] S. Sundaresan, K.G.K. Murti, The formation of intermetallic phases in aluminum–austenitic stainless steel friction welds, Material Forum 17 (1993) 301–307.
[4] M. Hansen, Constitution of Binary Alloys, McGraw-Hill Book Company, Inc, New York, 1958, pp. 91.
[5] K. Richter, G. Bostanjoglo, R. Dommaschk, R. Mayrhofer, D. Weber, H. Weber, Comparative study on aluminum and steel welding with cw and repetitively Q-switched Nd–YAG lasers, SPIE 2789 (12) (1996) 12–20.
[6] D.C. Weckman, H.W. Kerr, J.T. Liu, The effects of process variables on pulsed Nd:YAG laser spot welds: Part II. AA 1100 aluminum and comparison to AISI 409 stainless steel, Metallurgical and Materials Transactions B 28B (1997) 687–700.

[7] S. Fukumoto, T. Inuki, H. Tsubakino, K. Okita, M. Aritoshi, T. Tomital, Evaluation of friction weld interface of aluminum to austenitic stainless steel joint, Materials Science and Technology 13 (1997) 679–686.
[8] S. Fukumoto, M. Ohashi, H. Tsubakino, K. Okita, M. Aritoshi, T. Tomita, K. Goto, Microstructure of friction welded joint of 6061 aluminum alloy to 304 stainless steel, Journal of Japan Institute of Light Metals 48 (1998) 36–41.
[9] T.J. Lienert, J.R.W.L. Stellwag, B.B. Grimmett, R.W. Warke, Friction stir welding studies on mild steels, Welding Journal Supplement 82 (2003) 1S–9S.
[10] A.P. Reynolds, W. Tang, T. Gnaupel-Herold, H. Prask, Sturcture, properties, and residual stress of 304L stainless steel friction stir welds, Scripta Materialia 48 (2003) 1289–1294.
[11] T. Watanabe, H. Takawama, K. Kimapong, N. Hotta, Joining of steel to aluminum alloy by interface-activated adhesion welding, Materials Science Forum 426–432 (2003) 4129–4134.
[12] P.G. Shewmon, Transformations in Metals, first ed., McGraw-Hill, New York, NY, (1988) 93–97.
[13] ASM, Binary Alloy Phase Diagrams, second ed., 1996, CD-ROM.
[14] S. Fukumoto, H. Tsubakino, K. Okita, M. Aritoshi, T. Tomita, Amorphization by friction welding between 5052 aluminum alloy and 304 stainless steel, Scripta Materialia 42 (2000) 807–812.
[15] L.E. Murr, G. Liu, J.C. McClure, A TEM study of precipitation and related microstructures in friction-stir-welded 6061 aluminum, Journal of Material Science 33 (1998) 1243–1251.
[16] D. Dornfeld, Application of acoustic emission techniques in manufacturing, NDT and E International 25 (1999) 259–269.
[17] C.M. Chen, R. Kovacevic, D. Jandgric, Wavelet transform analysis of acoustic emission in monitoring friction stir welding of 6061 aluminum, International Journal of Machine Tools and Manufacture 43 (2003) 1383–1390.